

## Article

# Single-Micelle-Templated Synthesis of Hollow Barium Carbonate Nanoparticle for Drug Delivery

Bishnu Prasad Bastakoti <sup>1,\*</sup>, Nischal Bhattarai <sup>2</sup>, Moses D. Ashie <sup>1</sup>, Felix Tettey <sup>3</sup>, Shin-ichi Yusa <sup>4</sup>  
and Kenichi Nakashima <sup>5</sup>

<sup>1</sup> Department of Chemistry, North Carolina A & T State University, 1601 E Market St, Greensboro, NC 27411, USA

<sup>2</sup> Western Guilford High School, 409 Friendway Rd, Greensboro, NC 27410, USA

<sup>3</sup> Department of Industrial and Systems Engineering, North Carolina A & T State University, 1601 E Market St, Greensboro, NC 27411, USA

<sup>4</sup> Department of Applied Chemistry, University of Hyogo, 2167 Shosha, Himeji 671-2280, Japan

<sup>5</sup> Department of Chemistry, Faculty of Science and Engineering, Saga University, 1 Honjo-machi, Saga 840-8502, Japan

\* Correspondence: bpbastakoti@ncat.edu

**Abstract:** A laboratory-synthesized triblock copolymer poly(ethylene oxide-*b*-acrylic acid-*b*-styrene) (PEG-PAA-PS) was used as a template to synthesize hollow BaCO<sub>3</sub> nanoparticles (BC-NPs). The triblock copolymer was synthesized using reversible addition–fragmentation chain transfer radical polymerization. The triblock copolymer has a molecular weight of  $1.88 \times 10^4$  g/mol. Transmission electron microscopy measurements confirm the formation of spherical micelles with a PEG corona, PAA shell, and PS core in an aqueous solution. Furthermore, the dynamic light scattering experiment revealed the electrostatic interaction of Ba<sup>2+</sup> ions with an anionic poly(acrylic acid) block of the micelles. The controlled precipitation of BaCO<sub>3</sub> around spherical polymeric micelles followed by calcination allows for the synthesis of hollow BC-NPs with cavity diameters of 15 nm and a shell thickness of 5 nm. The encapsulation and release of methotrexate from hollow BC-NPs at pH 7.4 was studied. The cell viability experiments indicate the possibility of BC-NPs maintaining biocompatibility for a prolonged time.

**Keywords:** block copolymer; barium carbonate; hollow particles; drug delivery; micelles



**Citation:** Bastakoti, B.P.; Bhattarai, N.; Ashie, M.D.; Tettey, F.; Yusa, S.-i.; Nakashima, K. Single-Micelle-Templated Synthesis of Hollow Barium Carbonate Nanoparticle for Drug Delivery. *Polymers* **2023**, *15*, 1739. <https://doi.org/10.3390/polym15071739>

Academic Editors: Panagiotis Barmplexis and Konstantinos N. Kontogiannopoulos

Received: 6 March 2023

Revised: 17 March 2023

Accepted: 29 March 2023

Published: 31 March 2023



**Copyright:** © 2023 by the authors. Licensee MDPI, Basel, Switzerland. This article is an open access article distributed under the terms and conditions of the Creative Commons Attribution (CC BY) license (<https://creativecommons.org/licenses/by/4.0/>).

## 1. Introduction

BaCO<sub>3</sub> has attracted much research recently due to its many essential applications in producing pigments, catalysts, optical glass, and electric condensers [1–7]. Moreover, it is a precursor for producing magnetic ferroelectric, superconductors, and ceramic materials [8]. They are typically synthesized using the precipitation method [9–11]. Citric acid was used as a stabilizer to synthesize the BaCO<sub>3</sub> nanoparticles (BC-NPs). The primary function of citric acid is to provide a polymeric network to hinder cations' mobility, which reacts with Ba<sup>2+</sup> ions to form a metal ion–citric acid complex. The complex is a platform for the crystallization of BC-NPs. The pure orthorhombic crystal was obtained after calcining at 450 °C. The crystallite sizes increased with an increase in the calcination temperature [12]. Nagajyothi et al. synthesized BC-NPs in an aqueous extract of mango seed. The sub-20 nm mixed (spherical and triangular) structured nanoparticles were used to treat cervical carcinoma [13]. BaCO<sub>3</sub> is also used in tuning the optical properties of rare earth materials, which have wide applications in biomaterials, lasers, light-emitting diodes, and optical communication. It is considered as one of the favored host materials for lanthanide doping [14,15]. It brings new physical and chemical stability, high transparency, and good moisture resistance properties. Eu<sup>3+</sup>-doped BC-NPs were synthesized via the auto-combustion method [16]. The addition of the lanthanide ions did not change the structure and crystallinity; however, the optical properties of the composite were significantly improved.

Among the other morphologies, hollow nanostructures have attracted recent research interest due to their large pore volume, low mass density, and high surface-to-volume ratio compared to their solid counterparts [17–19]. Especially in bioapplication, the hollow void encapsulates the drug molecules and releases them when necessary [20]. The porous hollow shell is a diffusion barrier for the controlled release of payloads. Inorganic hollow nanoparticles are synthesized via various methods, such as soft templating, hard templating, and template-free methods [21,22]. The use of polymeric micelles as a template has proven to be a successful route toward synthesizing hollow structures with controllable size and morphology. We used a single-micelle templating method to synthesize the sub-50 nm hollow nanoparticles of metal, metal oxides, and metal phosphate [23–25]. In the recent report, a positively charged spherical micelle of poly(ethylene oxide-vinyl pyridine-styrene) (PEO-PVP-PS) block copolymer interacts with positively charged metal sources through a negatively charged phosphate ions bridge. After removing the polymer template via calcination, the hollow nanoparticles of nickel phosphate were obtained [26]. The dimension of the hollow void and shell thickness were easily tuned by controlling the molecular weight of the core and shell of the block copolymer [23,27].

The synthesis of  $\text{BaCO}_3$  nanoparticles with the hollow void is always difficult due to the fast precipitation reaction between  $\text{Ba}^{2+}_{(\text{aq})}$  ions and  $\text{CO}_3^{2-}_{(\text{aq})}$  ions. Here, we designed a polymer so that polymer micelles stabilize the BC-NPs. The reversible addition-fragmentation chain transfer (RAFT) radical polymerization was used to synthesize a triblock copolymer poly(ethylene oxide-*b*-acrylic acid-*b*-styrene) (PEG-PAA-PS).  $\text{Ba}^{2+}$  ions interact with the polyacrylic acid block to form a chelating complex that undergoes a selective precipitation reaction with carbonate on the PAA/ $\text{Ba}^{2+}$  ions shell. The interaction of metal ions with the polymer, the controlled precipitation of  $\text{BaCO}_3$ , and the formation of hollow structures were characterized by various techniques, including dynamic light scattering (DLS), Fourier-transform infrared (FTIR) spectroscopy, thermogravimetric analysis (TGA), transmission electron microscopy (TEM), and X-ray diffraction (XRD). The calcination of  $\text{BaCO}_3$ /polymer composites burns up the polymer, leaving the hollow void to encapsulate drug molecules and the porous shell as a diffusion barrier for controlled release (Figure 1). Finally, a cell proliferation assay was performed to check the biocompatibility of the nanoparticles to be used as drug carriers. As far as we have noticed, this is the first report on synthesizing sub-50 nm BC-NPs being used in drug delivery to date.

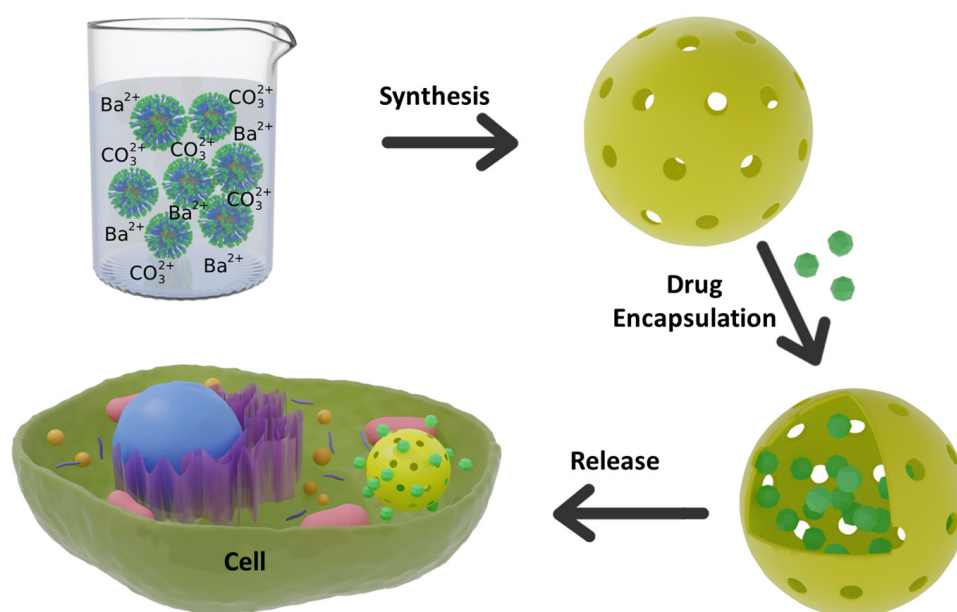


**Figure 1.** Synthesis of hollow  $\text{BaCO}_3$  nanoparticle and use of it as a drug carrier.

## 2. Materials and Methods

### 2.1. Materials

Poly(ethylene glycol) 4-cyano-4-(phenylcarbonothioylthio)pentanoate (PEG macro-CTA, average molecular weight =  $2.00 \times 10^3$  g/mol) from Aldrich (Tokyo, Japan) was used without further purification. 2,2'-Azobis(isobutyronitrile) (AIBN, >98%) from Wako pure chemical (Osaka, Japan) was recrystallized from methanol. Acrylic acid (AA, >99.0%), *N,N*-dimethylformamide (DMF, >99.5%), and 1,4-dioxane (>99.0%) from Tokyo Industry (Tokyo, Japan) were dried over 4 Å molecular sieves and distilled under reduced pressure. Styrene was washed with an aqueous alkaline solution and distilled from calcium hydride under reduced pressure. PEG-PAA-PS was synthesized (Figure 2) using RAFT polymerization as previously reported [25].  $\text{Na}_2\text{CO}_3$ ,  $\text{BaCl}_2 \cdot 2\text{H}_2\text{O}$ , and methotrexate were purchased from Thermo Scientific (Waltham, MA, USA). A 0.1 M tris buffer (solution of pH 7.4, EMD millipore corp.) was used as release media. Dulbecco's modified Eagle's medium (DMEM) and Dulbecco's phosphate-buffered saline (DPBS) were obtained from Life Technologies (Grand Island, NY, USA). Alamar Blue, lactate dehydrogenase (LDH) assay kit and every other materials not otherwise specified were purchased from Thermo Scientific.

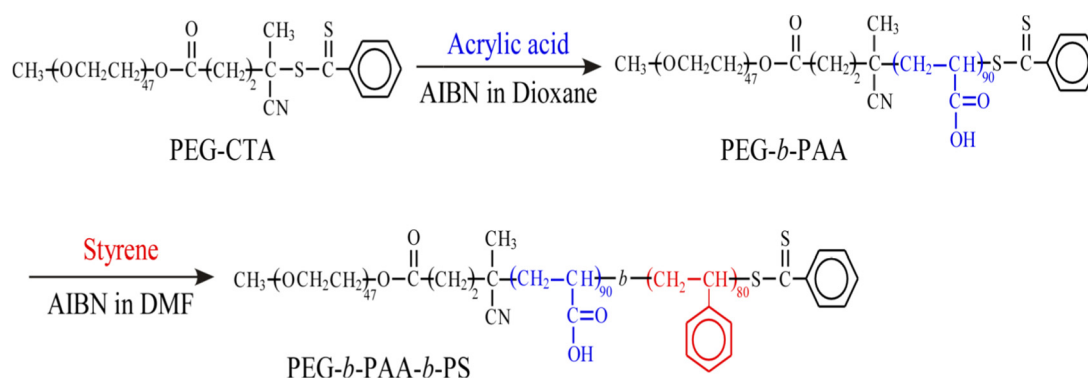


**Figure 2.** Synthesis of PEG-PAA-PS block copolymer via RAFT-controlled radical polymerization.

### 2.2. Synthesis of Block Copolymer

First, we prepared PEG-PAA diblock copolymer as follows. PEG macro-CTA (475 mg, 0.2 mmol,  $M_n(\text{NMR}) = 2.36 \times 10^3$  g/mol), AA (2.18 g, 30.3 mmol), and AIBN (12.5 mg, 0.08 mmol) were dissolved in 1,4-dioxane (95 mL) with a molar ratio of  $[\text{AA}]/[\text{PEG macro-CTA}]/[\text{AIBN}] = 151/1/0.38$ . The solution was purged with Ar gas for 30 min. Polymerization was carried out at 60 °C for 40 h under Ar gas. After polymerization, the obtained polymer was purified by dialysis against pure water for two days. The diblock copolymer (PEG-PAA) was recovered by a freeze-drying technique (1.7 g, 64.0%). Number-average degree of polymerization (DP) of the PAA block was estimated from  $^1\text{H}$  NMR spectrum in  $\text{DMSO}-d_6$  to be 90 (Figure S1). Number-average molecular weight ( $M_n(\text{NMR})$ ) for PEG-PAA was  $8.85 \times 10^3$  g/mol.  $M_n(\text{GPC})$  and molecular weight distribution ( $M_w/M_n$ ) were  $1.53 \times 10^4$  g/mol and 1.31, respectively (Figure S2), estimated from gel permeation chromatography (GPC). Styrene (10.4 g, 0.100 mol), AIBN (8.23 mg, 0.05 mmol), and PEG-PAA (1.11 g, 0.13 mmol,  $M_n(\text{theo}) = 8.85 \times 10^3$  g/mol) were dissolved in DMF (100 mL) with a molar ratio of  $[\text{styrene}]/[\text{PEG-PAA}]/[\text{AIBN}] = 798/1/0.40$ . The solution was degassed by purging with Ar gas for 30 min. The polymerization was carried out at 60 °C for 24 h. The conversion of styrene was 20.6%, determined from  $^1\text{H}$  NMR for the polymerization mixture. The polymerization mixture was poured into a large excess of ethyl acetate. The precipitate was dialyzed against tetrahydrofuran for three days and pure water for a day. The triblock copolymer (PEG-PAA-PS) was recovered by a freeze-drying technique (2.06 g, 19.8%). DP of the PS block was 80 as estimated by  $^1\text{H}$  NMR in  $\text{DMSO}-d_6$  at 100 °C.  $M_n(\text{NMR})$  for the triblock copolymer was  $1.88 \times 10^4$  g/mol (Figure S3). We could not perform GPC

measurements for PEG-PAA-PS because the polymer can molecularly dissolve only in DMSO at high temperatures.

### 2.3. Preparation of Polymeric Micelle and Synthesis of BaCO<sub>3</sub> Nanoparticles

A total of 20 mg of the polymer was dissolved in 10 mL of tetrahydrofuran. The solution was sonicated for 20 min and magnetically stirred for 12 h. The solution was dialyzed against water to prepare an aqueous solution of the polymer. The final concentration of polymer was made to be 0.1 g/L<sup>-1</sup> at pH 9. A total of 20 mg barium chloride was added to 20 mL of a micelle solution (0.1 g/L<sup>-1</sup>) and stirred for 1 h. A total of 8.8 mg of sodium carbonate was added to the mixture, leaving 2 h for precipitation reaction. The BaCO<sub>3</sub>/polymer composite particles were recovered by centrifugation. The composite particles were thoroughly washed with deionized water and dried in an oven at 50 °C before calcination at 550 °C for 3 h at a ramping rate of 2 °C min<sup>-1</sup>.

### 2.4. Characterization

The kinetics and progress of the polymerization reaction were studied using a Bruker DRX-500 nuclear magnetic resonance (NMR) spectrometer operating at 500 MHz and gas permeation chromatography (GPC). A refractive index (RI) detector equipped with a Shodex GF-7M HQ column working at 40 °C and a flow rate of 0.6 mL/min was used in the GPC measurement of PEG-PAA. A phosphate buffer (pH 8) containing 10 vol % acetonitrile was used as the eluent. The instrument was calibrated using the sodium poly(styrene sulfonate) standard. The dynamic light scattering measurements were carried out using an Otsuka ELS Z zeta potential and particle analyzer. All of the measurements were carried out at 25 °C and filtered through a 0.4 µm cellulose filter. The concentration and pH of the solution was maintained at 0.1 g/L and 9, respectively. The hydrodynamic diameter ( $D_h$ ) was calculated using Stokes–Einstein equation ( $D_h = k_B T / 3\pi\eta D$ ). Here,  $k_B$  is the Boltzmann constant,  $T$  is the absolute temperature,  $D$  is the diffusion coefficient, and  $\eta$  is the solvent viscosity. The zeta potential ( $\zeta$ ) was calculated from the Smolichowski equation ( $\mu_E = \zeta\epsilon/\eta$ ).  $\mu_E$  is electrophoresis mobility and  $\epsilon$  is the permittivity of the solvent. The TEM measurements were carried out using a JEOL JEM-1210 electron microscope at an accelerating voltage of 80 kV. The hollow barium carbonate nanoparticles were dispersed into ethanol and cast on the copper grid for TEM measurement. For polymeric micelles, phosphotungstic acid was used as a contrasting agent. The crystallinity and phase identification of the hollow nanoparticles was carried out using a Shimadzu-630D X-ray diffractometer at 40 kV, 30 mA, and with CuK $\alpha$  radiation (1.5406 Å). A simultaneous thermogravimetric analysis (TGA) and a differential thermal analysis (DTA) were carried out using a SEIKO-6300 TG/DTA instrument at a heating rate of 10 °C min<sup>-1</sup> in air. FTIR data were collected from the IR Tracer-100 in attenuated total reflection mode (Shimadzu, Kyoto, Japan).

### 2.5. Drug Release

A total of 50 mg of BC-NPs was dispersed into 2.5 mL of 4 mM methotrexate drug solution. The solution was sonicated for 60 min and magnetically stirred for 24 h in the dark for equilibration. A dialysis cassette was wetted for 2 min before sample injection. The equilibrated drug solution was injected into the cassette, ensuring no air bubbles. The cassette was diagonally placed in a beaker containing 100 mL of tris buffer solution of pH 7.4. The buffer (release medium) was stirred at a constant rate of 100 rpm at room temperature. A 3 mL solution from the beaker was sampled, and the absorbance of methotrexate was taken. The sample solution was returned to vessels after every reading. In the controlled experiment, 2.5 mL of 4 mM methotrexate drug solution was injected into the cassette and the release phenomenon without using nanoparticles was studied.

## 2.6. Cell Preparation

NIH-3T3 cells (a mouse fibroblast cell line, ATCC 1658) were maintained in standard DMEM supplemented with 10% FBS, 1% pen strip, and 0.12% insulin. The cells were cultured in 75 cm<sup>2</sup> tissue culture flasks at 37 °C in a 5% CO<sub>2</sub> humidified environment. Cells were trypsinized using 0.25% trypsin/EDTA at 80% confluence. Trypsinized cells formed pellets when centrifuged and were re-suspended in fresh media at the required cell density. The experiment utilized passage number eight cells.

## 2.7. Toxicity Study

The BC-NPs were first exposed under UV light for 12 h and were suspended in sterile deionized water by sonication for 30 min. To make different exposure solutions (e.g., 0, 50, 100, and 500 µg mL<sup>-1</sup>), the BC-NPs solution was added to the DMEM medium containing 10% FBS and was thoroughly mixed via vortexing. The BC-NPs solutions were labeled as BC-0, BC-50, BC-100, and BC-500. The BC-0 sample, which has no BC-NPs, represents the control sample, whereas BC-50 to 500 represents the different amounts of NPs used. The cells were treated with 1 mL of the different concentrations of BC-NPs according to a previous publication [28]. Cells treated with the different concentrations of BC-NPs solutions were cultured at 37 °C in a 5% CO<sub>2</sub> humidified environment. At specific time points (24 h, 48 h, and 72 h), the supernatant of the cell–particle medium was collected and stored for cytotoxicity study. The cytotoxicity effect of the BC-NPs on the fibroblast cells was determined using the Pierce lactate dehydrogenase (LDH) cytotoxicity assay kit as described in our earlier publication [29,30]. Briefly, 50 µL of each stored sample was transferred to a 96-well flat-bottom plate and triplicated. Next, 50 µL of the reaction mixture generated from the protocol was added to each sample well, and the plate was kept in the dark for 30 min at room temperature. The positive and negative controls were established based on the manufacturer’s kit protocol. The reaction mixture kept in the dark was stopped by adding 50 µL of stop solution to each sample well and mixed by gentle tapping. The absorbance of the assay solution in the well plate was measured at 490 nm and 680 nm using a CLARIOstar<sup>®</sup> multi-mode plate reader (BMG LABTECH Inc., Cary, NC, USA). The cytotoxicity was then calculated using the following equation:

$$\text{Cytotoxicity} = \frac{\text{OD at 490 nm test sample} - \text{OD at 490 nm negative control}}{\text{OD at 490 nm positive sample} - \text{OD at 490 nm negative control}} \times 100\% \quad (1)$$

where OD is absorbance.

## 2.8. Cell Viability Study

3T3 cells were observed with an Alamar Blue (AB) colorimetric assay according to the manufacturer’s standard protocol [31]. For this assay, the medium was removed from the cells treated with BC-NPs after being washed twice with PBS and then incubated for four hours with 5% (v/v) AB reagent in the respective culture medium (50 µL of AB reagent in 1 mL culture medium). Assay solutions were transferred to fresh plates, and multiple aliquots were taken to measure fluorescence on a microplate reader (CLARIOstar Plus, BMG LABTECH Inc., Cary, NC, USA) with excitation at 530 nm and emission at 590 nm. Cell viability was calculated using the following equation:

$$\text{Cell Viability} = \frac{\text{Fluorescence of the sample} - \text{Fluorescence of the blank}}{\text{Fluorescence of the control} - \text{Fluorescence of the blank}} \times 100\% \quad (2)$$

All results were expressed as mean ± SD. Data were analyzed for significance with OriginPro Version 2023 software (Origin Lab, Northampton, MA, USA).

## 2.9. Fluorescence Imaging and Analysis

Fluorescence imaging of the 3T3 fibroblast cells with BC-NPs was completed as previously reported [29]. Briefly, the excess medium was removed, and samples were washed twice with DPBS and then stained with 15 µL of acridine orange (AO) and propidium iodide

(PI) nucleic acid binding dyes (Nexcelom Bioscience, Lawrence, MA, USA) and incubated at 37 °C for 10 min. Images were photographed under an Olympus IX83 microscope using Olympus cell Sens Dimension software (Olympus Corporation, Shinjuku, Tokyo, Japan).

### 3. Results and Discussion

The polymer was first dissolved in THF and collected in water by dialysis. The exchange of THF with water makes the solution slightly turbid, indicating the formation of micelles. The Tyndall effects on the polymer solution confirm to the formation of colloidal nanoaggregates (Figure S4). The dynamic light scattering experiment shows that the hydrodynamic diameter ( $D_h$ ) of the micelles is 74 nm (Figure 3). The zeta potential of the polymer solution at pH 9 is  $-28$  mV. We believe that the polyacrylic acid chains exhibit fully extended conformation as the solution pH is higher than the  $pK_a$  (4.5) value of acrylic acid [32]. The advantage of these micelles (negatively charged) is that the positively charged metal ions strongly bind electrostatically. The addition of  $Ba^{2+}$  ions turns the solution slightly more turbid, indicating an increased hydrophobicity of  $Ba^{2+}$ /PEG-PAA-PS nanoaggregates (Figure S4). The  $D_h$  of  $Ba^{2+}$ /PEG-PAA-PS decreases to 43 nm, suggesting a decrease in electrostatic repulsion among PAA units due to the neutralization of the negative charge of PAA with  $Ba^{2+}$  ions. The increase in the zeta potential from  $-28$  mV to  $-3$  mV after the addition of metal ions further confirms the masking of the negative charge of micelles by positively charged metal ions. The block copolymer is expected to form uniform spherical micelles in an aqueous solution with the PEG corona, PAA shell, and PS core. After staining with phosphotungstic acid, nanoaggregates were observed by TEM, and spherical micelles were obtained. This provides concrete evidence of the formation of micelles in water. The white sphere indicates a negatively stained PS core (Figure 4a). The micelles' size (30 nm) from TEM is much smaller than that from DLS (74 nm). This discrepancy is due to the different modes of measurement. DLS is a solution-based measurement. The water around the micelles helps to expand their size. The hydrophilic parts (PEG and deprotonated PAA) have a fully extended form. However, TEM measurement is performed in dry and high vacuum conditions. The micelles are dry and shrunken, which makes the size obtained from TEM always smaller than that of DLS.

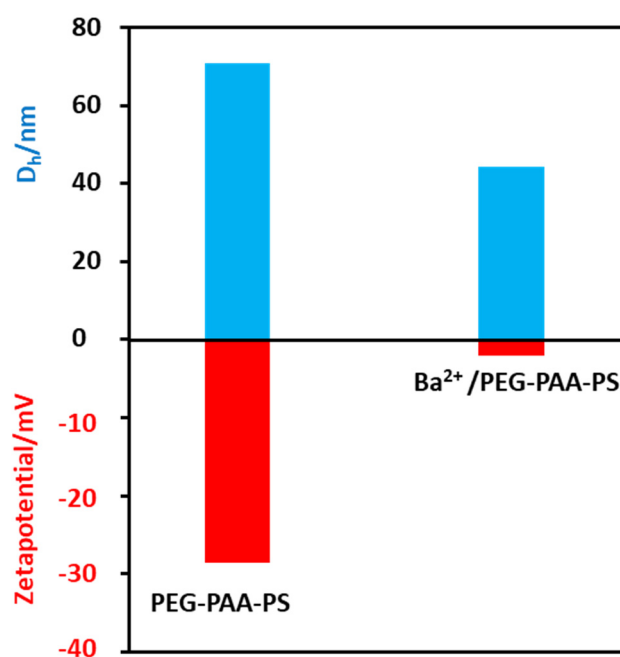


**Figure 3.** Hydrodynamic diameter ( $D_h$ ) and zeta potential of pure polymeric micelles and micelles composites.

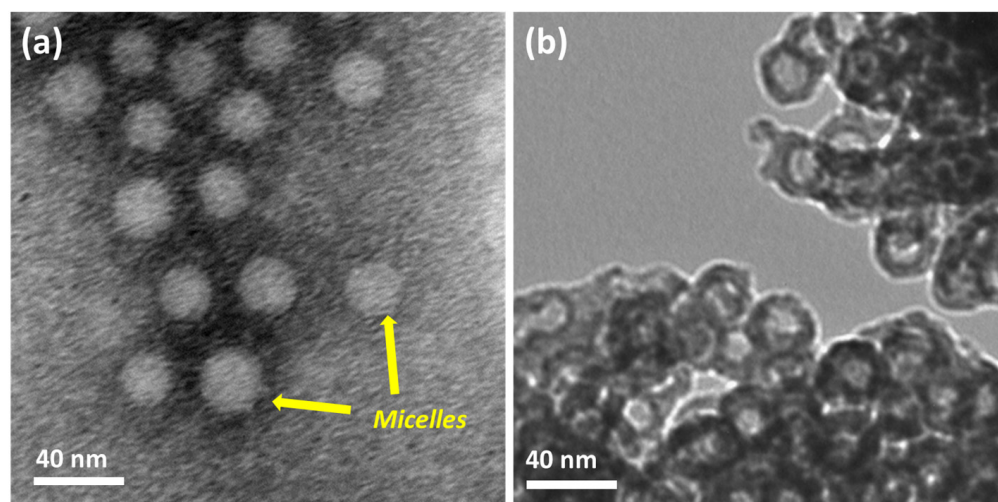


**Figure 4.** TEM images of (a) polymeric micelles and (b) hollow BaCO<sub>3</sub> nanoparticles.

Polymeric micelles are widely used as a template and structure-directing agent for synthesizing hollow nanoparticles with controllable dimensions. Nakashima et al. synthesized silica nanosphere templating on PEO-PVP-PS block copolymer [33]. The controlled polymerization of silica precursors with the micelles template allows for fabricating hollow nanospheres with different shell thicknesses and hollow voids. The addition of Ba<sup>2+</sup> ions into a micelles solution forms a chelating complex with PAA blocks. One of the most exciting applications of the PEG-PAA-PS micelles in this study is a template for synthesizing inorganic hollow particles of BaCO<sub>3</sub>. Ba<sup>2+</sup> ions first interact with micelles electrostatically.

The precipitation of BaCO<sub>3</sub> occurs around the Ba<sup>2+</sup>/PEG-PAA-PS nanoaggregates to form BaCO<sub>3</sub>/PEG-PAA-PS nanocomposites. The removal of the polymeric template by calcination led to the formation of hollow BC-NPs (Figure 4b). The cavity diameter is approximately 15 nm, with a thickness of 5 nm. The void diameter is smaller than the size of the PS core. This happens because the materials shrink during calcination at high temperatures. It is not easy to synthesize the sub-50 nm hollow nanoparticles due to the extremely fast kinetics of the formation of BaCO<sub>3</sub>. Salvatori et al. studied the nucleation and growth rate of BaCO<sub>3</sub> [34]. The particles formed are generally micron-sized. Specific additives, such as block copolymers, strongly influence nucleation, growth, and self-organization [35]. The use of a triblock copolymer made the method easy and opened the avenue to synthesizing hollow structures with controllable dimensions. The slight weight loss at the initial part of the thermogravimetric analysis curves is due to the desorption of absorbed water molecules (Figure 5a). The strong exothermic peaks on the differential thermal analysis (DTA) curves around 400 °C show the thermal decomposition of the template polymer. The high carbon content and higher thermal stability of the polymer suppress the unwanted crystal growth at higher temperatures. The higher weight loss after 850 °C and a large endothermic peak on the DTA curve is possibly attributed to the decomposition of the BaCO<sub>3</sub> crystal. FTIR confirmed the formation of BaCO<sub>3</sub> nanoparticles (Figure 5b). The sharp peaks at 692 cm<sup>-1</sup> and 856 cm<sup>-1</sup> are the in-plane and out-of-plane bending of the CO<sub>3</sub><sup>2-</sup> ion. The 1415 cm<sup>-1</sup> band corresponds to the asymmetric stretching mode of C-O, and the weak band at 1060 cm<sup>-1</sup> is attributed to the symmetric C-O stretching vibration. The crystalline characteristics of the obtained BC-NPs were confirmed by XRD analysis. The sharp diffraction peaks (Figure S5) of the sample indicate that well-crystallized BC-NPs were obtained under the current synthetic conditions. No characteristic peaks due to impurities were detected, indicating that the BaCO<sub>3</sub> nanoparticles are of high purity.

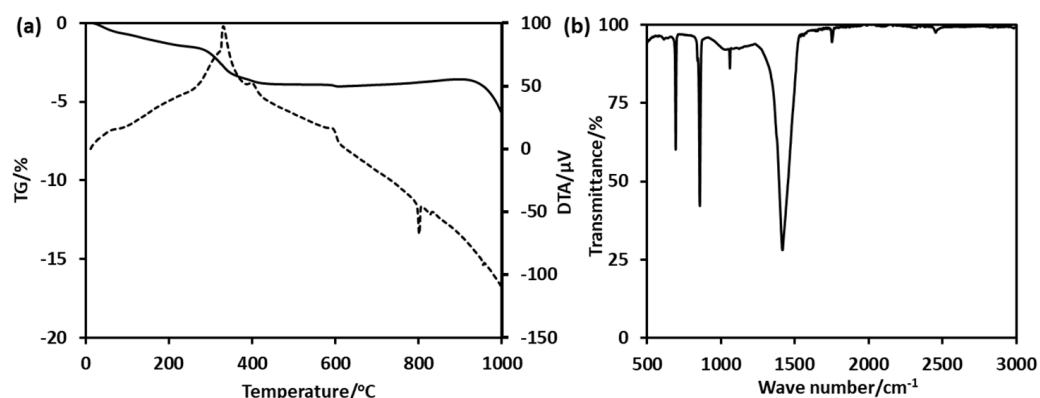


**Figure 5.** (a) Thermogravimetric analysis (TGA) results of BaCO<sub>3</sub>/PEG-PAA-PS nanocomposites and (b) Fourier transform infrared (FTIR) spectrum of hollow BaCO<sub>3</sub> nanoparticles.

The 3T3 fibroblast cells were treated with different concentrations of BC-NPs (BC-0, BC-50, BC-100, and BC-500) for up to three days, as shown in Figure 6. In evaluating the in vitro cytotoxic activity of BC-NPs, we observed no significant difference in LDH release among all of the tested samples on day 1. However, the highest induced BC-NPs (BC-500) showed a considerable amount of LDH release on day 3, which translates to its toxicity, and thus the substantial dead cells representation in the fluorescence image in Figure 7. The sample with the least BC-NPs (BC-50) resulted in the least LDH release overall. The cell proliferation assay using Alamar Blue (Figure 6b) shows that the cell viability remains relatively unchanged in all of the tested samples except for the sample with the concentration of nanoparticles increased to 500  $\mu\text{g mL}^{-1}$ , which showed cell viability deterioration on day 2 and more significantly on day 3. These findings are comparable with previously reported literature [28]. The cell viability graph indicates the possibility of BC-NPs maintaining biocompatibility after day 3, mainly for the BC-50 and possibly BC-100-induced samples. However, a perfect sample amount recommendation will be the BC-50, which satisfies cell compatibility even after day 3 and can further be evaluated and implemented in the future for biomedical applications.

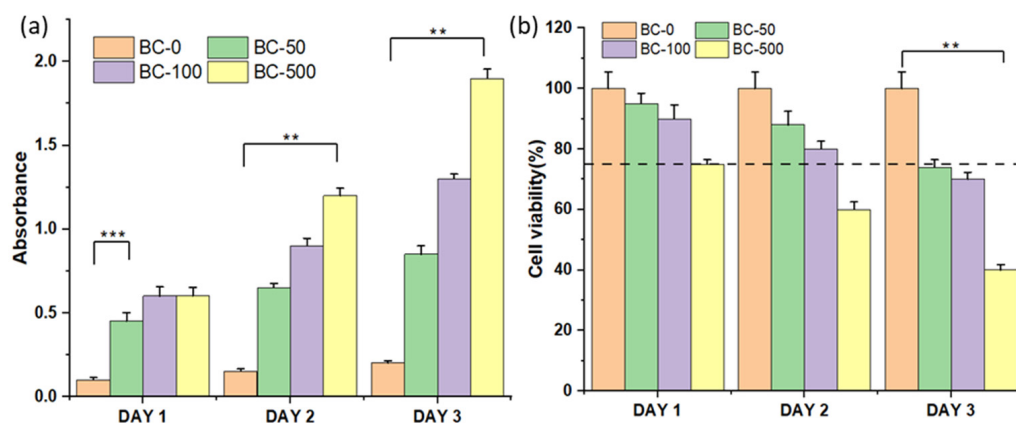


**Figure 6.** (a) Cytotoxicity graph and (b) cell viability graph of the BC-NPs with the 3T3 fibroblast cells ( $n = 3$ ), where \*\* represents  $p < 0.01$  and \*\*\* represents  $p < 0.001$ .

The hollow nanoparticles have several advantages for drug delivery due to the high surface-to-volume ratio, porosity, and large void that can accommodate a large number of drug molecules to be delivered. Silica-based materials have been widely used as drug carriers. It has been reported that doxorubicin-loaded hollow nanoparticles were taken up by cancer cell lines and released the drug into the tumor. The growth rate was better reduced compared to the case where the free drug was introduced [36]. We investigated

the release pattern of methotrexate from hollow BC-NPs at pH 7.4 using the dialysis method. First, the drug was encapsulated into the hollow nanoparticles and released from the hollow nanoparticles to the bulk aqueous phase inside the dialysis cassette. Then, it diffused to the aqueous phase outside the dialysis tube. The amount of the released drug was monitored outside of the dialysis membrane spectrophotometrically. The absorbance of methotrexate was recorded at 375 nm. It was observed that the drugs were released sustainably without burst release (Figure S6). We showed the drug release profile without using nanoparticles for comparison. In the first three hours, the release rate was similar for the hollow nanoparticles and the controlled experiment. This may be due to the loosely bound drug molecules on the surface of  $\text{BaCO}_3$  hollow nanoparticles. However, at the later stage, the drug molecules were released more slowly from the hollow nanoparticles than in the controlled condition. Hybridizing  $\text{BaCO}_3$  with other materials such as  $\text{SiO}_2$ ,  $\text{TiO}_2$ , and  $\text{Fe}_2\text{O}_3$  or functionalizing nanoparticles with stimuli responsive polymer would control the drug loading and release phenomena [37–39].

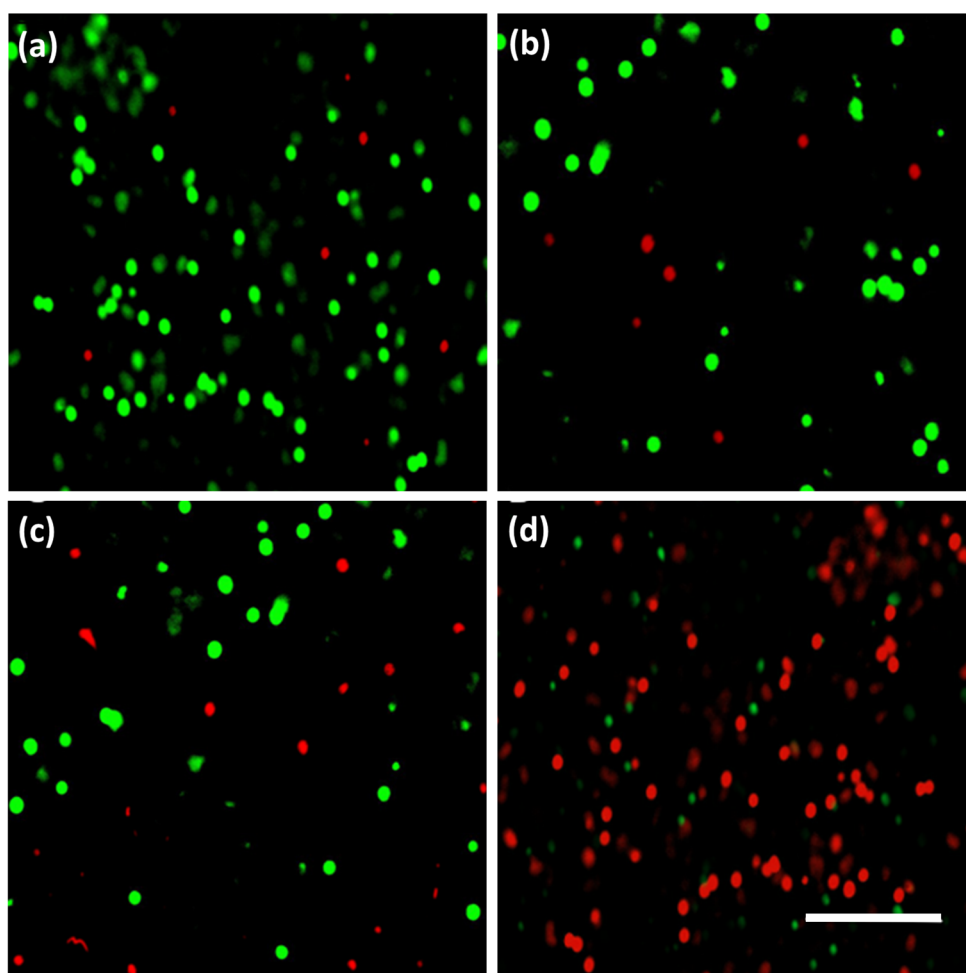


**Figure 7.** Fluorescence image showing live (green) and dead (red) cells of 3T3 fibroblast cells after exposure to different concentrations of BC-NPs at day 3. BC-0 (a), BC-50 (b), BC-100 (c), and BC-500 (d). All images were taken at  $20\times$  magnification. The scale bar is  $100\ \mu\text{m}$ .

#### 4. Conclusions

$\text{BaCO}_3$  hollow nanoparticles were synthesized using a laboratory-designed triblock copolymer. RAFT-controlled radical polymerization allows for the synthesis of the block copolymer with the desired molecular weight. The triblock copolymer PEG-PAA-PS undergoes self-assembly to form spherical micelles with three chemically distinct domains in an aqueous solution. The hydrophobic PS core is a template used to generate a hollow

void. The negatively charged PAA shell plays a vital role in arresting  $\text{Ba}^{2+}$  ions for the selective precipitation of  $\text{BaCO}_3$  on the shell region of the micelles. The hydrophilic PEG provides stability to the polymer–inorganic composite nanostructures after the precipitation reaction of  $\text{BaCO}_3$ . The removal of the polymeric portion of the nanocomposites at high temperatures gives rise to hollow nanoparticles of  $\text{BaCO}_3$ , proving that the polymeric system could be an excellent template for fabricating the hollow nanoparticles of inorganic materials undergoing a fast precipitation reaction. The in vitro release of methotrexate from the hollow particles shows that 64% of the drugs were released after 5.5 h. The encapsulated drug release was slower than the free drug molecules. However, the release kinetics are identical at the early stage, showing that drug molecules are loosely adsorbed on the surface of  $\text{BaCO}_3$  nanoparticles. Making composites or a suitable functionalization of  $\text{BaCO}_3$  nanoparticles would allow for the control of drug release kinetics. In addition, the obtained BC-NPs exhibit a very high biocompatibility, showing great promise for intracellular bio-applications in the future.

**Supplementary Materials:** The following supporting information can be downloaded at: <https://www.mdpi.com/article/10.3390/polym15071739/s1>, Figure S1.  $^1\text{H}$  NMR for PEG-PAA in  $\text{DMSO-d}_6$  at  $100^\circ\text{C}$ . Figure S2. GPC elution curve for PEG-PAA using phosphate buffer as an eluent at  $40^\circ\text{C}$ . Figure S3.  $^1\text{H}$  NMR for PEG-PAA-PS in  $\text{DMSO-d}_6$  at  $100^\circ\text{C}$ . Figure S4: Tyndal effect showing the formation of colloidal particles: (a) PEG-PAA-PS polymer, (b)  $\text{Ba}^{2+}$ /PEG-PAA-PS (c)  $\text{BaCO}_3$ /PEG-PAA-PS aqueous solutions. Figure S5: XRD spectrum of hollow  $\text{BaCO}_3$  nanoparticles. Figure S6: Drug release profile from hollow  $\text{BaCO}_3$  nanoparticles.  $A_t$  and  $A_\infty$  are the absorbance of the released drug at time  $t$  and infinity, respectively.

**Author Contributions:** Conceptualization, B.P.B., S.-i.Y. and K.N.; methodology, N.B., M.D.A. and F.T.; validation, N.B., M.D.A. and F.T.; investigation, N.B., M.D.A., F.T. and B.P.B. resources, B.P.B.; writing—original draft preparation, N.B., M.D.A. and F.T.; writing—review and editing, B.P.B., S.-i.Y. and K.N.; supervision, B.P.B., S.-i.Y. and K.N.; project administration, B.P.B.; funding acquisition, B.P.B. All authors have read and agreed to the published version of the manuscript.

**Funding:** B.P.B. thanks the National Science Foundation Research Initiation Award (2000310) and Excellence in Research Award (2100710) USA.

**Institutional Review Board Statement:** Not applicable.

**Data Availability Statement:** Data will be made available on request.

**Acknowledgments:** B.P.B. thanks the National Science Foundation Research Initiation Award (2000310) and Excellence in Research Award (2100710) USA. The authors thank Narayan Bhattarai for the discussion of the cell experiment, and Albert Bastakoti for the illustration.

**Conflicts of Interest:** The authors declare no conflict of interest.

## References

1. Fan, X.; Deng, L.; Li, K.; Lu, H.; Wang, R.; Li, W. Adsorption of malachite green in aqueous solution using sugarcane bagasse-barium carbonate composite. *Colloids Interface Sci. Commun.* **2021**, *44*, 100485. [[CrossRef](#)]
2. Andel-Gawwad, H.A.; Mewally, K.A.; Tawfik, T.A. Role of barium carbonate and barium silicate nanoparticles in the performance of cement mortar. *J. Build. Eng.* **2021**, *44*, 102721. [[CrossRef](#)]
3. Rahmat, R.; Halima, N.; Heryanto, H.; Sesa, E.; Tahir, D. Improvement X-ray radiation shield characteristics of composite cement/Titanium dioxide ( $\text{TiO}_2$ )/Barium carbonate ( $\text{BaCO}_3$ ): Stability crystal structure and chemical bonding. *Radiat. Phys. Chem.* **2023**, *204*, 110634. [[CrossRef](#)]
4. Dilip, R.; Jayaprakash, R.; Sangaiya, P.; Gopi, S. The magnetic property alterations due to transition from barium ferrite ( $\text{BaFe}_2\text{O}_4$ ) nano rods to barium carbonate ( $\text{BaCO}_3$ ) quantum dots. *Results Mater.* **2020**, *7*, 100121. [[CrossRef](#)]
5. Zhang, W.; Zhang, F.; Ma, L.; Yang, J.; Yang, J.; Xiang, H. Prediction of the crystal size distribution for reactive crystallization of barium carbonate undergrowth and nucleation mechanisms. *Cryst. Growth Des.* **2019**, *19*, 3616–3625. [[CrossRef](#)]
6. Cao, X.; Hong, T.; Yang, R.; Tian, J.-H.; Xia, C.; Dong, J.-C.; Li, J.-F. Insights into the catalytic activity of barium carbonate for oxygen reduction reaction. *J. Phys. Chem. C* **2016**, *120*, 22895–22902. [[CrossRef](#)]
7. He, Y.; Yanf, B.; Cheng, G.; Pan, H. Synthesis of  $\text{La}_2\text{O}_3/\text{BaCO}_3$  nanocatalysts and their catalytic performance. *Powder Technol.* **2003**, *134*, 52. [[CrossRef](#)]

8. Tsuzuku, K.; Couzi, M. In situ investigation of chemical reactions between BaCO<sub>3</sub> and anatase or rutile TiO<sub>2</sub>. *J. Mater. Sci.* **2012**, *47*, 4481. [[CrossRef](#)]
9. Yu, S.-H.; Colfen, H.; Xu, A.-W.; Dong, W. Complex Spherical BaCO<sub>3</sub> superstructures self-assembled by a facile mineralization process under the control of simple polyelectrolytes. *Cryst. Growth Des.* **2004**, *4*, 33. [[CrossRef](#)]
10. Guo, X.-H.; Yu, S.-H. Controlled mineralization of barium carbonate mesocrystals in a mixed solvent and at the air/solution interface using a double hydrophilic block copolymer as a crystal modifier. *Cryst. Growth Des.* **2007**, *7*, 354. [[CrossRef](#)]
11. Li, W.; Sun, S.; Yun, Q.; Wu, P. Controlling the morphology of BaCO<sub>3</sub> aggregates by carboxymethyl cellulose through polymer induced needle-stacking self-assembly. *Cryst. Growth Des.* **2010**, *10*, 2685–2692. [[CrossRef](#)]
12. Zelati, A.; Amirabadizadeh, A.; Kompany, A. Complex Preparation and characterization of barium carbonate nanoparticles. *Int. J. Chem. Eng. Appl.* **2011**, *2*, 1.
13. Nagajyothi, P.C.; Pandurangan, M.; Sreekanth, T.V.M.; Shim, J. In vitro anticancer potential of BaCO<sub>3</sub> nanoparticles synthesized via green route. *J. Photochem. Photobiol. B Biol.* **2016**, *156*, 29. [[CrossRef](#)]
14. Gu, J.; Bian, Z.; Yin, B.; Jin, C.; Liu, X.; Gao, Y.; Wu, J.; Tanf, S.; Gao, F.; Zhao, Y.S. Simultaneous structure and luminescence property control of barium carbonate nanocrystals through small amount of lanthanide doping. *Sci. Bull.* **2017**, *62*, 1239. [[CrossRef](#)]
15. Tripathi, G.; Rai, V.K.; Rai, S.B. Spectroscopic studies of Eu<sup>3+</sup> doped calibo glass: Effect of the addition of barium carbonate, energy transfer in the presence of Sm<sup>3+</sup>. *Opt. Commun.* **2006**, *264*, 116. [[CrossRef](#)]
16. Abidine, B.; Yahya, M.; Mhadhbi, M.; Bouzidi, C.; Hamzaoui, A.H. Characterization and luminescence properties of Eu<sup>3+</sup> doped BaCO<sub>3</sub> nanoparticles synthesized by autocombustion method. *J. Mol. Struct.* **2022**, *1263*, 133122. [[CrossRef](#)]
17. Munkaila, S.; Dahal, R.; Kokayi, M.; Jackson, T.; Bastakoti, B.P. Hollow structured transition metal phosphates and their applications. *Chem. Rec.* **2022**, *22*, e202200084. [[CrossRef](#)]
18. Bastakoti, B.P.; Guragain, S.; Yokoyama, Y.; Yusa, S.; Nakashima, K. Synthesis of hollow CaCO<sub>3</sub> nanospheres templated by micelles of poly(styrene-*b*-acrylic acid-*b*-ethylene glycol) in aqueous solutions. *Langmuir* **2011**, *27*, 379–384. [[CrossRef](#)]
19. Yasun, E.; Gandhi, S.; Choudhary, S.; Mohammadinejad, R.; Benyettou, F.; Gozubenli, N.; Arami, H. Hollow micro and nanostructures for therapeutic and imaging applications. *J. Drug Deliv. Sci. Technol.* **2020**, *60*, 102094. [[CrossRef](#)]
20. Chang, Z.; Yang, Y.; Zhao, B.; Li, H.; Guan, Y.; Zhao, Y.; Yuan, H.; Ni, C. Dual-targeting magnetic fluorescent mesoporous organosilicon hollow nanospheres for gambogic acid loading, sustained release and anti-tumor properties. *J. Mol. Liq.* **2022**, *360*, 119412. [[CrossRef](#)]
21. Bastakoti, B.P.; Li, Y.; Kimura, T.; Yamauchi, Y. Asymmetric block copolymers for supramolecular templating of inorganic nanospace materials. *Small* **2015**, *11*, 1992. [[CrossRef](#)] [[PubMed](#)]
22. Sun, L.; Lv, H.; Feng, J.; Guselnikova, O.; Wang, Y.; Yamauchi, Y.; Liu, B. Noble-Metal-Based Hollow Mesoporous Nanoparticles: Synthesis Strategies and Applications. *Adv. Mater.* **2022**, *34*, 2201954. [[CrossRef](#)] [[PubMed](#)]
23. Li, Y.; Bastakoti, B.P.; Malgras, V.; Li, C.; Tang, J.; Kim, J.H.; Yamauchi, Y. Polymeric micelle assembly for the smart synthesis of mesoporous platinum nanospheres with tunable pore sizes. *Angew. Chem.* **2015**, *127*, 11225. [[CrossRef](#)]
24. Li, Y.; Bastakoti, B.P.; Yamauchi, Y. Research Update: Triblock copolymers as templates to synthesize inorganic nanoporous materials. *APL Mater.* **2016**, *4*, 040703. [[CrossRef](#)]
25. Guragain, S.; Bastakoti, B.P.; Ito, M.; Yusa, S.; Nakashima, K. Aqueous polymeric micelles of poly [N-isopropylacrylamide-*b*-sodium 2-(acrylamido)-2-methylpropanesulfonate] with a spiropyran dimer pendant: Quadruple stimuli-responsiveness. *Soft Matter* **2012**, *8*, 9628. [[CrossRef](#)]
26. Bastakoti, B.P.; Munkaila, S.; Guragain, S. Micelles template for the synthesis of hollow nickel phosphate nanospheres. *Mater. Lett.* **2019**, *251*, 34–36. [[CrossRef](#)]
27. Bastakoti, B.P.; Ishihara, S.; Leo, S.Y.; Ariga, K.; Wu, K.C.W.; Yamauchi, Y. Polymeric micelle assembly for preparation of large-sized mesoporous metal oxides with various compositions. *Langmuir* **2014**, *30*, 651. [[CrossRef](#)]
28. Raessi, M.; Alijani, H.Q.; Nematollahi, F.F.; Baty, R.S.; Batiha, G.E.-S.; Khan, A.U.; Hashemi, N.; Iravani, S.; Sharifi, I.; Aflatoonian, M.; et al. Barium carbonate nanostructures: Biosynthesis and their biomedical applications. *Ceram. Int.* **2021**, *47*, 21045. [[CrossRef](#)]
29. Khanal, S.; Bhattarai, S.R.; Sankar, J.; Bhandari, R.K.; Macdonald, J.M.; Bhattarai, N. Nano-fibre integrated microcapsules: A nano-in-micro platform for 3D cell culture. *Sci. Rep.* **2019**, *9*, 1. [[CrossRef](#)]
30. Tatum, S.D.; Saudi, S.; Tettey, F.; Bhandari, R.K.; Bhattarai, N. A Novel hydrogel-bronchial epithelial cell spheroids for toxicological evaluation. *Biomed. Sci. Instrum.* **2021**, *57*, 4. [[CrossRef](#)]
31. Bhattarai, S.R.; Saudi, S.; Khanal, S.; Aravamudhan, S.; Rorie, C.J.; Bhattarai, N. Electrodynamically assisted self-assembled fibrous hydrogel microcapsules: A novel 3D in vitro platform for assessment of nanoparticle toxicity. *RSC Adv.* **2021**, *11*, 4921. [[CrossRef](#)] [[PubMed](#)]
32. Swift, T.; Swanson, L.; Geoghegan, M.; Rimme, S. The pH-responsive behavior of poly(acrylic acid) in aqueous solution is dependent on molar mass. *Soft Matter* **2016**, *12*, 2542. [[CrossRef](#)] [[PubMed](#)]
33. Khanal, A.; Inoue, Y.; Yada, M.; Nakashima, K. Synthesis of silica hollow nanoparticles templated by polymeric micelle with core-shell-corona structure. *J. Am. Chem. Soc.* **2007**, *129*, 1534. [[CrossRef](#)] [[PubMed](#)]
34. Salvatori, F.; Muhr, H.; Plasari, E.; Bossoutrot, J.-M. Determination of nucleation and crystal growth kinetics of barium carbonate. *Powder Technol.* **2002**, *128*, 114. [[CrossRef](#)]

35. Luccio, T.D.; Laera, A.M.; Tapfer, L.; Kempter, S.; Kraus, R.; Nickel, B. Controlled nucleation and growth of CdS nanoparticles in a polymer matrix. *J. Phys. Chem. B* **2006**, *110*, 12603. [[CrossRef](#)]
36. Wang, T.; Chai, F.; Fu, Q.; Zhang, L.; Liu, H.; Liao, Y.; Su, Z.; Wang, C.; Duan, B.; Ren, D. Uniform hollow mesoporous silicananocages for drug delivery in vitro and in vivo for liver cancer therapy. *J. Mater. Chem.* **2011**, *21*, 5299. [[CrossRef](#)]
37. Ardiansyah, A.; Rahmat, R.; Azlan, M.; Heryanto, H.; Tahir, D. Nanocrystal composites cement/BaCO<sub>3</sub>/Fe<sub>2</sub>O<sub>3</sub> for improved X-ray shielding characteristics: Stability structural properties. *J. Mat. Res.* **2022**, *37*, 4114. [[CrossRef](#)]
38. Buscaglia, M.T.; Buscaglia, V.; Alessio, R. Coating of BaCO<sub>3</sub> crystals with TiO<sub>2</sub>: versatile approach to the synthesis of BaTiO<sub>3</sub> tetragonal nanoparticles. *Chem. Mater.* **2007**, *19*, 711. [[CrossRef](#)]
39. Zhu, W.; Cai, C.; Lin, J.; Chen, L.; Zhuang, Z. Polymer micelles-directed growth of BaCO<sub>3</sub> spiral nanobelts. *Chem. Commun.* **2012**, *48*, 8544. [[CrossRef](#)]

**Disclaimer/Publisher's Note:** The statements, opinions and data contained in all publications are solely those of the individual author(s) and contributor(s) and not of MDPI and/or the editor(s). MDPI and/or the editor(s) disclaim responsibility for any injury to people or property resulting from any ideas, methods, instructions or products referred to in the content.